frontiers | Frontiers in Cell and Developmental Biology

TYPE Original Research
PUBLISHED 28 December 2023
DOI 10.3389/fcell.2023.1293420

OPEN ACCESS

EDITED BY
Mariano F. Zacarias-Fluck,
Vall d'Hebron Institute of Oncology (VHIO), Spain

REVIEWED BY
Leonie M. Quinn,
Australian National University, Australia
Lorenzo Montanaro,
University of Bologna, Italy

*CORRESPONDENCE
Paola Bellosta,
paola.bellosta@unitn.it

†These authors have contributed equally to this work

RECEIVED 13 September 2023
ACCEPTED 29 November 2023
PUBLISHED 28 December 2023

CITATION
Manara V, Radoani M, Belli R, Peroni D, Destefanis F, Angheben L, Tome G, Tebaldi T and Bellosta P (2023), NOC1 is a direct MYC target, and its protein interactome dissects its activity in controlling nucleolar function. *Front. Cell Dev. Biol.* 11:1293420. doi: 10.3389/fcell.2023.1293420

NOC1 is a direct MYC target, and its protein interactome dissects its activity in controlling nucleolar function

Valeria Manara[1†], Marco Radoani[1†], Romina Belli[1†], Daniele Peroni[1†], Francesca Destefanis[1,2], Luca Angheben[1], Gabriele Tome[1], Toma Tebaldi[1,3] and Paola Bellosta[1,4*]

[1]Department of Computational, Cellular, Integrative Biology CIBIO, University of Trento, Trento, Italy, [2]Institute of Evolutionary Biology CSIC Universitat Pompeu Fabra, Barcelona, Spain, [3]Department of Internal Medicine, Yale School of Medicine, New Haven, CT, United States, [4]Department of Medicine, NYU Langone Medical Center, New York, NY, United States

The nucleolus is a subnuclear compartment critical in ribosome biogenesis and cellular stress responses. These mechanisms are governed by a complex interplay of proteins, including NOC1, a member of the NOC family of nucleolar proteins responsible for controlling rRNA processing and ribosomal maturation. This study reveals a novel relationship between NOC1 and MYC transcription factor, known for its crucial role in controlling ribosomal biogenesis, cell growth, and proliferation. Here, we demonstrate that NOC1 functions as a direct target of MYC, as it is transcriptionally induced through a functional MYC-binding E-box sequence in the NOC1 promoter region. Furthermore, protein interactome analysis reveals that NOC1-complex includes the nucleolar proteins NOC2 and NOC3 and other nucleolar components such as Nucleostemin1 Ns1 transporters of ribosomal subunits and components involved in rRNA processing and maturation. In response to MYC, NOC1 expression and localization within the nucleolus significantly increase, suggesting a direct functional link between MYC activity and NOC1 function. Notably, NOC1 over-expression leads to the formation of large nuclear granules and enlarged nucleoli, which co-localize with nucleolar fibrillarin and Ns1. Additionally, we demonstrate that NOC1 expression is necessary for Ns1 nucleolar localization, suggesting a role for NOC1 in maintaining nucleolar structure. Finally, the co-expression of NOC1 and MYC enhances nucleolus size and maintains their co-localization, outlining another aspect of the cooperation between NOC1 and MYC in nucleolar dynamics. This study also reveals an enrichment with NOC1 with few proteins involved in RNA processing, modification, and splicing. Moreover, proteins such as Ythdc1, Flacc, and splenito are known to mediate N6-methyladenosine (m6A) methylation of mRNAs in nuclear export, revealing NOC1's potential involvement in coordinating RNA splicing and nuclear mRNA export. In summary, we uncovered novel roles for NOC1 in nucleolar homeostasis and established its direct connection with MYC in the network governing nucleolar structure and

function. These findings also highlight NOC1's interaction with proteins relevant to specific RNA functions, suggesting a broader role in addition to its control of nucleolar homeostasis and providing new insight that can be further investigated.

KEYWORDS

NOC1, MYC, E-box, nucleolus, mass spectrometry, interactome

1 Introduction

MYC is a transcription factor crucial in the regulation of factors controlling ribosomal biogenesis and protein synthesis, which occurs primarily through its ability to regulate the transcription of genes required for ribosome assembly and function (van Riggelen et al., 2010; Campbell and White, 2014; Destefanis et al., 2020). MYC promotes the transcription of its target genes, such as ribosomal proteins and co-factors, by binding to specific DNA sequences known as E-boxes (5′-CACGTG-3′) within their promoter region (Fernandez et al., 2003; Orian et al., 2003; Hulf et al., 2005). MYC also promotes the transcription of ribosomal RNA (rRNA) genes, which are transcribed by RNA polymerase I to generate the precursor rRNA transcripts. Since ribosomes are central to protein synthesis and cell growth, MYC's role in promoting ribosomal biogenesis largely contributes to protein synthesis, necessary for cell growth and proliferation, a function that is conserved both in flies and vertebrates (Schlosser et al., 2003; Arabi et al., 2005; Grandori et al., 2005; Grewal et al., 2005; Van Riggelen et al., 2010; Destefanis et al., 2020).

NOC1 is a nucleolar protein that, together with NOC2 and NOC3, plays a critical role in the maturation of rRNA and the transport of the pre-ribosomal subunits (Sailer et al., 2022; Dorner et al., 2023). NOC1 in yeast works as a heterodimer with NOC2 during the initial maturation of the ribosomal RNA (rRNA) and in the transport of the pre-60S ribosomal subunit, a process that is completed by NOC2/NOC3 heterodimers (Milkereit et al., 2001). Studies on the distribution of affinity-tagged NOC1 and, more recently, proteomics and crosslinking coupled to mass spectrometry, confirmed the presence of NOC1 in the early pre-60S complex (Sailer et al., 2022; Dorner et al., 2023), while cryo-EM studies showed its role in the formation of heterodimers with NOC2, essential for the quality-control checkpoint of the maturation of the large ribosome subunit (Sanghai et al., 2023).

We recently characterized NOC1 function in flies and showed its role in controlling polysome abundance, rRNA maturation, protein synthesis, and cell survival (Destefanis et al., 2022). Furthermore, lowering NOC1 levels in different contexts, such as whole animals or specific organs, results in various developmental and functional impairments (Destefanis et al., 2022). Our initial transcriptomic analysis revealed NOC1 as a potential direct target of MYC (Hulf et al., 2005); thus, we further analyzed this critical function in the context of ribosomal biosynthesis directed by MYC.

Here, we show that NOC1 is a direct transcriptional target of MYC, and its activation is mediated by a functional E-box sequence located in the promoter region of the *NOC1* gene. We then used HA-NOC1 as bait to perform Mass Spectrometry (MS) analysis to determine the NOC1 interactome to characterize NOC1 function and connect its activity with biological processes, mainly focusing on components that control nucleolar homeostasis.

Bioinformatic analysis using the STRING database identified clusters of NOC1 protein interactors, and the most significant was on ribosome biogenesis. These data showed a significative enrichment of NOC2 and NOC3 ($p < 0.05$) strongly aligning with data published previously in yeast (Milkereit et al., 2001; Hierlmeier et al., 2013), and a significant cluster of nucleolar proteins, such as fibrillarin (fib) and nucleostemin 1 (Ns1), and others, like Novel nucleolar proteins (Non1 and Non3) and mushroom body miniature (mbm), involved in the 60S subunit biogenesis. Moreover, we found an enrichment of nucleolar and nuclear proteins, like Nnp (Hulf et al., 2005), and peter pan (ppan) (Migeon et al., 1999; Zielke et al., 2022), involved in pre-rRNAs production and RNA maturation, and modulo (mod) (Perrin et al., 2003), that were previously identified as direct targets of MYC, emphasizing the relation between NOC1 and MYC.

In addition, these studies also identified enrichment of the nuclear m^{6}A "reader" YTH domain RNA Binding Protein C1 (Ythdc1) (Roundtree et al., 2017), Flacc (Fl(2)d-associated protein), and spenito (nito) (Knuckles et al., 2018). Remarkably, these proteins are part of the complex that mediates the N6-Methyladenosine methylation of mRNAs for their nuclear export (Knuckles et al., 2018; Shi et al., 2021). We could outline a novel function for the MYC-NOC1 axis in regulating mRNA m^{6}A modification and transport.

Finally, the observation that NOC1 controls the nucleolar localization of Ns1, together with those indicating that MYC enhances NOC1-induced large granular structures in the nucleus, further sustains the functional relationship between MYC and NOC1 in maintaining nucleolar homeostasis.

In summary, these findings will provide significant insights into the role of NOC1 and its interactome that may contribute to the control of nucleolar functions, supporting the crucial role of MYC in regulating growth, proliferation, and protein synthesis.

2 Materials and methods

2.1 Fly stocks and husbandry

Fly cultures and crosses were raised at 25°C on a standard medium containing 9 g/L agar (ZN5 B and V), 75 g/L corn flour, 60 g/L white sugar, 30 g/L brewers' yeast (Fisher Scientific), 50 g/L fresh yeast and 50 mL/L molasses (Naturitas), along with nipagin and propionic acid (Fisher). The lines used were obtained by: *UAS-HA-MYC* (*Bellosta et al., 2005*); *NOC1-GFP* (*B51967*) *UAS-NOC1-HA* (Flyorf-CH) *NOC1-RNAi* (B25992). *UAS-Ns1-GFP* is a gift from Patrick J. Di Mario University of Louisiana, LA). *hsp70-Gal4* gift from Florenci Serras (University of Barcelona, Spain).

2.2 Cloning NOC1 E-box and molecular biology

Site-directed mutagenesis (SDM) was carried out using the following primers for the mutant E-box 5′ TTC GGC ACG AGT TTG AAT AGA ATT CCG AGT TGT TTC TAA CGC CG; 5' CGG CGT TAG AAA CAA CTC GGA ATT CTA TTC AAA CTC GTG CCG AA; following instructions from the SDM kit (Promega). Promoter elements used in luciferase reporter expression analyses were cloned into the pGL3-basic vector (Promega).

2.3 Cell culture and luciferase assays

S2 *Drosophila* cells were propagated in Schneider's *Drosophila* medium (Gibco), supplemented with 10% fetal bovine serum, at 24°C. S2 cell transfections were carried out using Cellfectin (Invitrogen). *NOC1* reporter constructs were added at 1 µg per 10^6 cells; tubulin- Renilla luciferase control DNA were co-transfected at 0.1 µg per 10^6 cells and incubated with a transfection mix for 12 h. Cells were harvested 24 or 60 h posttransfection. Relative gene expression was determined using the Dual-Luciferase Reporter assay system (Promega) on a luminometer.

2.4 RNA extraction and quantitative RT-PCR analysis

Total RNA was extracted from 8 whole larvae using the QIAGEN RNeasy Mini Kit (Qiagen) according to the manufacturer's instructions. Extracted RNAs were quantified using an ultraviolet (UV) spectrophotometer, and RNA integrity was confirmed with ethidium bromide staining. 1 µg total RNA from each genotype was reverse transcribed into cDNA using SuperScript IV MILO Master Mix (Invitrogen). The obtained cDNA was used as the template for quantitative real-time PCR (qRT-PCR) using qPCR Mastermix (Promega). mRNAs expression levels were normalized to *actin-5C mRNA* used as the internal control. The relative level for each gene was calculated using the 2-DDCt method (Hulf et al., 2005) and reported as arbitrary units. Three independent experiments were performed and cDNAs were used in triplicate. The following primers were used for qRT-PCR: *Actin5c:* 5′CAGATC ATGTTCGAGACCTTCAAC; 5′ACGACCGGAGGCGTACAG (Parisi et al., 2013).

Fibrillarin: 5′ACGACAGTCTCGCATGTGTC; 5′ATGCGG TACTTGTGTGGATG (this work).

MYC: 5′CATAACGTCGACTTGCGTG; 5′GAAGCTCCCTGC TGATTTGC (Parisi et al., 2013).

NOC1: 5′CTATACGCTCCACCGCACAT; 5′GTCGCTACC GAACTTGTCCA (Destefanis et al., 2022).

2.5 Protein extractions and Western blotting

Five larvae for each genotype were lysed in 200 µL of lysis buffer (50 mM Hepes/pH 7.4, 250 mM NaCl, 1 mM (EDTA), 1.5% Triton X-100 containing a cocktail of phosphatases inhibitors (PhosSTOP 04906837001, Merck Life Science) and proteases inhibitors (Roche, cOmplete Merck Life Science). Samples were sonicated three times for 10 s using a Branson Ultrasonic Sonifier 250 (Branson, Darbury, CA, United States) equipped with a microtip set at 25% power. Tissue and cell debris were removed by centrifugation at 100,00× *g* for 30 min at 4°C. Proteins in the crude extract were quantified by a bicinchoninic acid (BCA) Protein assay Reagent Kit (Pierce), following the manufacturer's instructions with bovine serum albumin as the standard protein. For SDS-PAGE, samples were incubated for 8 min at 100°C in standard reducing 1x loading buffer; 40 µg of total protein were run on an SDS-polyacrylamide gel and transferred onto nitrocellulose membranes (GE-Healthcare, Fisher Scientific Italia) After blocking in 5% (*w*/*v*) non-fat milk in tris-buffered saline (TBS)-0.05% Tween (TBS-T), membranes were incubated overnight with primary antibodies: rat monoclonal anti-HA (1:1000, ROCHE), or Actin5c (1:200, #JL20) from Developmental Studies Hybridoma Bank (DSHB), University of Iowa, IA, United States. Appropriate secondary antibody was incubated for 2 h at room temperature, followed by washing. The signal was revealed with ChemiDoc Touch Imaging System (Bio-Rad Lab).

2.6 Immunoprecipitation

Hsp70 (hs)-Gal4> NOC1 larvae or control *hs-Gal4> w^{1118}* were heat-shocked at 37°C for 1 h and left to recover for 2 h at room temperature. 20 larvae from each genotype were washed in PBS and lysed with 750 µL of immunoprecipitation buffer (100 mM HEPES, 100 mM NaCl, 0.5% Triton, 10 mM MgCl) containing proteases and phosphatases inhibitors. Protein lysates were incubated for 20 min in ice and centrifuged at 13.000 rpm for 30 min a 4 °C. 500 µL of lysates were incubated with 50 µL of Sepharose-beads-Protein-G (Invitrogen) previously incubated with 4 µL anti-HA antibodies. Incubation was performed for 2 h at room temperature, and beads were washed extensively with ice cold lysing buffer. After centrifugation, bound proteins were eluted with 100 µL of SDS-loading buffer LDS Sample Buffer (Thermo Fisher Scientific) containing 5% Bolt Sample reducing agent (Thermo Fisher Scientific) at 80°C for 5 min 20 µL of the sample was run on a Western blot and 80 µL were used for the MS analysis. Experiments were repeated twice.

2.7 Mass spectrometry and proteomic interaction partners analysis

Immunoprecipitated samples were loaded on 10% SDS-PAGE and run for about 1 cm. Gels were then stained with Coomassie and the entire stained area was excised as one sample. Excised gel bands were cut into small plugs (~1 mm^3), rinsed with 50 mM ammonium bicarbonate and acetonitrile (ACN) solution, and vacuum dried. Dried gel pieces were then reduced using 10 mM DTT (56°C for 30 min) and alkylated using 55 mM iodoacetamide (room temperature for 30 min, in the dark). After sequential washing with 50 mM NH4HCO3 and ACN, gel pieces were dried and rehydrated with 12.5 ng/mL trypsin (Promega, Madison, WI) solution in 25 mM ammonium bicarbonate on ice for 30 min.

The digestion was continued at 37°C overnight. The tryptic peptides were sequentially extracted from the gels with 30% ACN/3% TFA and 100% ACN. All of the supernatants were combined and dried in a SpeedVac. The tryptic peptides were resuspended in 0.1% TFA, desalted on C18 stage tips, and resuspended in 20 µL of 0.1% formic acid buffer.

For LC-MS/MS analysis, the peptides were separated on an Easy-nLC 1200 UHPLC system (Thermo Fisher Scientific) using an 85-min gradient on a 25 cm long column (75 µm inner diameter) filled in-house with C18-AQ ReproSil-Pur material (3 µm particle size, Dr. Maisch, GmbH). The gradient was set as follows: from 5% to 25% in 52 min, from 25% to 40% in 8 min, and from 40% to 98% in 10 min, with a flow rate of 400 nL/min. The buffers were 0.1% formic acid in water (A) and 0.1% formic acid in acetonitrile (B). The peptides were analyzed with an Orbitrap Fusion Tribrid mass spectrometer (Thermo Fisher Scientific, San Jose, CA, United States) in data-dependent mode. Full scans were performed in the Orbitrap mass analyzer at a resolving power of 120,000 FWHM (at 200 m/z) in the mass range of 350–1,100 m/z, with a target value of 1×10^6 ions and a maximum injection time of 50 ms. Each full scan was followed by a series of MS/MS scans (collision-induced dissociation) over a cycle time of 3 s, with a maximum injection time of 150 ms (ion trap) and a target of 5×10^3 ions. The ion source voltage was set at +2,100 V and the ion transfer tube was warmed up to 275°C. Data was acquired using Xcalibur 4.3 and Tune 3.3 software (Thermo Fisher Scientific). QCloud was used for all acquisitions to control instrumental performance during the project, using quality control standards (Chiva et al., 2018).

For data and computational analysis, the raw files were searched in Proteome Discoverer version 2.2 software (Thermo Fisher Scientific). Peptide searches were performed using the UniProt *Drosophila melanogaster* (fruit-fly) database digested *in silico* (downloaded in July 2022) and a database containing common contaminants. Trypsin was chosen as the enzyme with 5 missed cleavages. The static modification of carbamidomethylation (C) was incorporated in the search, with variable modifications of oxidation (M) and acetylation (protein N-term). The MASCOT search engine (v.2.2 Matrix Science) was used to identify the proteins, using a precursor mass tolerance of 10 ppm and a product mass tolerance of 0.6 Da. False discovery rate was filtered for <0.01 at PSM, at peptide and protein levels. Results were filtered to exclude potential contaminants and proteins with less than two peptides.

MS downstream analysis was performed using the ProTN proteomics pipeline (www.github.com/TebaldiLab/ProTN and www.rdds.it/ProTN) (manuscript in preparation). Peptide intensities were log2 transformed, normalized (median normalization), and summarized into proteins (median sweeping) with functions in the DEqMS Bioconductor package (Zhu et al., 2020). Imputation of the missing intensities was executed by PhosR package (Kim et al., 2021). Differential analysis was performed with the DEqMS package, proteins with absolute log2 FC > 0.75 and *p*-value <0.05 were considered significant.

Protein-protein interaction network was constructed using STRING interaction database, version 12.0 (https://string-db.org/) (von Mering et al., 2003). Medium confidence interactions (score>0.4) were accepted as determined by the STRING database. The PPI network was grouped into relevant protein clusters using the Markov Cluster Algorithm (inflation parameter, 3) clustering option provided by STRING.

2.8 Immunostaining

Dissected tissues were fixed in 4% paraformaldehyde (PFA) (Electron Microscopy Science) in PBS for 30 min at room temperature. After permeabilization with 0.3% Triton/PBS, tissues were washed in Tween 0.04% in PBS, saturated with 1% BSA in PBS, and incubated overnight with anti-fibrillarin antibodies (1:100), anti-HA (1:100, ROCHE), anti-GFP (1:200, ThermoFisher A11122) and anti-MYC affinity-purified antibodies (1:1000) (Galletti et al., 2009; Destefanis et al., 2022). Relative secondary antibodies conjugated with Alexa555 and Alexa488 were used 1:2,000 (Invitrogen). After washing with PBST, samples were mounted on slides using Vectashield (Vector Laboratories) and fluorescence images were acquired using a Leica-TCS-SP8 confocal microscope.

3 Results

3.1 NOC1 contains a functional E-box sequence in its promoter region and is transcriptionally induced by MYC

Our initial observation on the transcriptomic analysis of potential MYC target genes identified NOC1 as a predicted nucleolar gene that contains in its 5′promoter region the E-box sequence CACGTG typically within the first 100 bp from the initial translation initiation codon ATG (Figure 1A), and thus considered a *bona-fide* MYC binding region (Hulf et al., 2005). By qRT-PCR, we show that constitutive expression of MYC in whole *Drosophila* larvae (Figure 1B) using the *actin* promoter resulted in NOC1 transcriptional activation and also in the upregulation of *fibrillarin-mRNA* (Figure 1C), a known MYC target that contains functional E-boxes in its promoter region conserved both in flies and vertebrates (Orian et al., 2003; Hulf et al., 2005; Koh et al., 2011).

The 5′promoter region of NOC1 contains a putative TATA box sequence at about - 26 bp from the transcription start, a sequence identified as the Transcription Start Site (TSS), and the CACGTG sequence (E-box) at −82 bp from the ATG transcription start (Figure 1A). To investigate whether the CACGTG sequence responds to MYC activation, we cloned the 5′promoter region of *NOC1*, containing the wildtype CACGTG sequence or the scramble sequence GAATTC (Figure 1D), upstream of a plasmid expressing the Firefly luciferase ORF. The reporter plasmids were co-transfected into *Drosophila* S2-MT-MYC cells with a plasmid expressing the Renilla luciferase. MYC expression was induced by adding CuSO4 to the medium (Figure 1E). Firefly luciferase activity was measured in the cell lysates after 5 h of induction and normalized to the co-transfected Renilla luciferase expressed under the control of the constitutive tubulin promoter (Figure 1F). As shown upon MYC expression, cells expressing the *NOC1* promoter region with the mutated E-box have significantly reduced luciferase activity compared to that from cells expressing the wild-type *NOC1* promoter, indicating that the

10.3389/fcell.2023.1293420

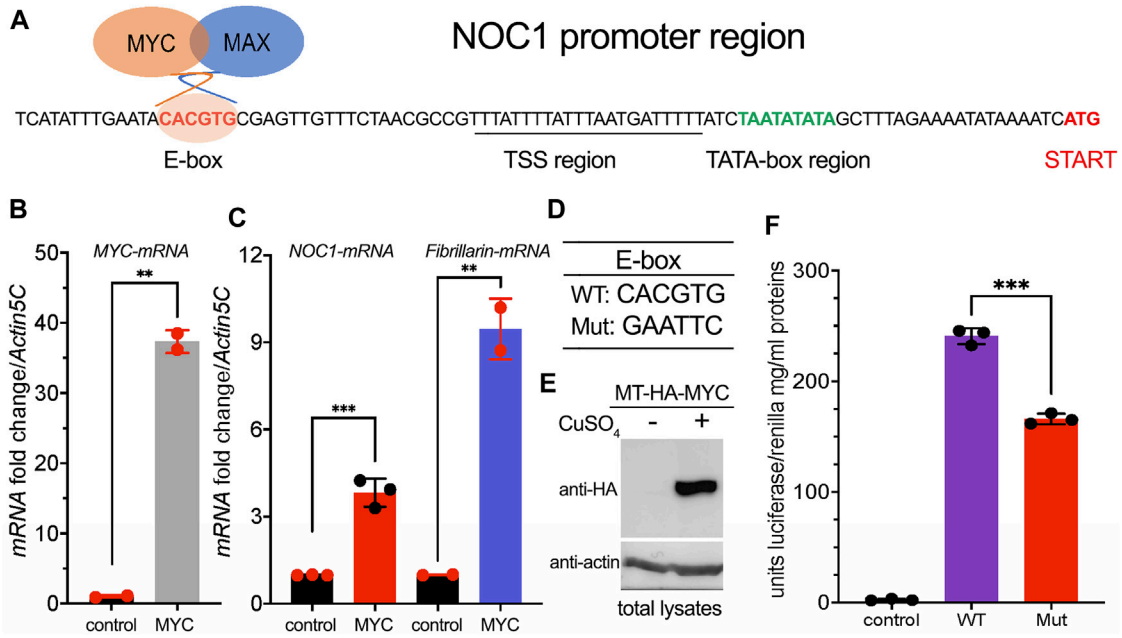

FIGURE 1
NOC1 contains in its promoter a functional MYC E-box sequence. **(A)** DNA promoter region of the *NOC1* gene showing the position of the E-box, the putative Transcription Start Sequence (TSS) with the TATA box, and the Initiation of Transcription point (START). **(B)** qRT-PCR from third instar whole larvae tissues showing the upregulation of *MYC-mRNA* **(B)** and of *NOC1* and *fibrillarin-mRNAs* **(C)** upon MYC induction. The expression of *UAS-MYC* was induced using the *actin-Gal4* promoter. **(D)** DNA sequences of WT and Mutant E-boxes. **(E)** Western blot from S2-MT-HA-MYC cells showing the expression level of the metallothionein HA-MYC upon induction for 5 h using $CuSO_4$. Actin was used as a control for loading. **(F)** Units of relative luciferase activity in lysates of S2-MT-HA-MYC cells treated for 5 h with $CuSO_4$ and transfected with Renilla plasmid alone (control), of with NOC1 promoter region containing WT (WT) or Mutant (Mut) E-box.

sequence CACGTG in the *NOC1* promoter functions as an enhancer of MYC activity.

3.2 Interactome analysis of NOC1 associates its expression with NOC2 and NOC3 proteins and other components of the nucleolus

To investigate how NOC1 might regulate nucleolus functions, we explored its binding partners by analyzing the total interactome through immunoprecipitation and tandem mass spectrometry analysis (Figure 2A). Third-instar larvae expressing *UAS-HA-NOC1* under the *actin-Gal4* were used first to test a few conditions to efficiently extract NOC1 protein from the cells (Figure 2B). As shown in the left panel, NOC1 is efficiently expressed in lysates from third-instar larvae as a 120 KDa protein detected by the anti-HA antibodies. We first tested three conditions for lysing the tissues to avoid high detergent and salt concentrations according to previous protocols for immunoprecipitation in whole larvae (Bellosta et al., 2005). The comparative analysis of the three lysis conditions led to selecting the buffer containing 0.5% Triton and 200 mM NaCl, which appears to balance mild stringency conditions and high recovery yield, making it suitable for extracting NOC1 protein in our experimental conditions (Figure 2; middle panel). Since we found NOC1 transcriptionally upregulated as early as 3 h upon MYC expression (Hulf et al., 2005) and (Figure 1C), we decided to use the inducible promoter *hsp70 (heat-shock)-Gal4* to ubiquitously express NOC1 to perform our analysis at a similar time point. *Hs-Gal4; UAS-HA-NOC1* larvae and control (*hs-Gal4; w^{1118}*) were heat-shocked for 1 hour and 37 °C. After 2 hours of recovery at room temperature, larvae were lysed to pursue the immunoprecipitation (IP) using anti-HA antibodies. Immunoblotting analysis showed enrichment of HA-NOC1 bands in the expected samples (Figure 2; left panel). While a weak band of 120 KDa is also visible in the control sample, the lower molecular weight bands characteristic of the NOC1 pattern are not present (Destefanis et al., 2022), confirming the specificity of the experiment.

To discover NOC1 protein partners, we used affinity purification coupled with label-free mass spectrometry (AP-MS). Specifically, we performed the co-immunoprecipitation of the tagged-NOC1 protein in *hs-Gal4; UAS-HA-NOC1* lysates, and the control tissues *hs-Gal4; w^{1118}*, respectively. Immunoprecipitates (IPs) were then analyzed by LC-MS/MS using an Easy-nLC 1200 UHPLC system coupled to an Orbitrap Fusion™ mass spectrometer. For protein identification and quantification, acquired raw data were imported into the Proteome Discoverer 2.2 (PD) platform and searched with MASCOT (v2.6 Matrix Science, London, United Kingdom) against the UniProtKB *Drosophila melanogaster* database. The quantitative output of PD was then further processed using the ProTN pipeline, enabling comprehensive quality control, statistical analysis, and interpretation of proteomic datasets. We identified a total of 239 proteins that were significantly ($p < 0.05$) enriched in HA-NOC1 immunoprecipitated (IPs) relative to control, representing

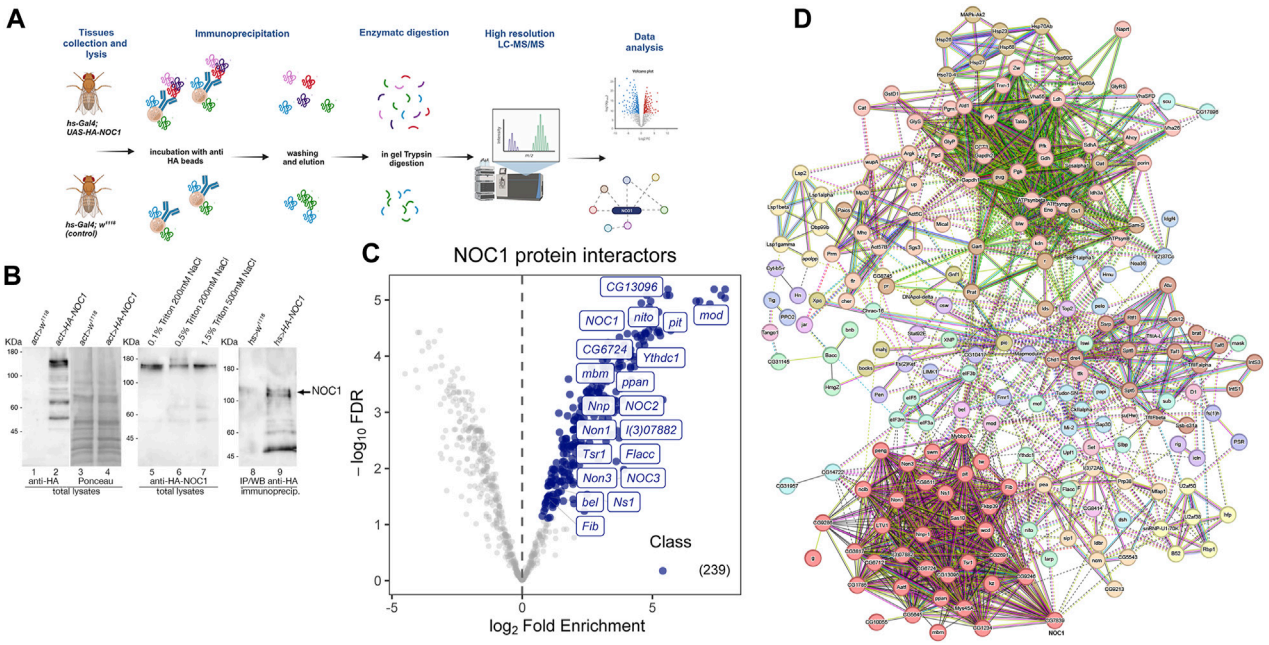

FIGURE 2
NOC1 is associated with components of the nucleolus. **(A)** Schematic representation of the workflow used to identify NOC1 interacting proteins. *hs-Gal4; UAS-HA-NOC1* larvae and control (*hs-Gal4; w*^{1118}) were lysed and subjected to immunoprecipitation using anti-HA conjugated beads. NOC1 immunoprecipitated proteins were eluted with Laemmli sample buffer and processed by *in-gel trypsin* digestion before MS/MS analysis. The figure is created with BioRender.com. **(B)** Western blot showing the expression of *UAS-HA-NOC1* in lysates from third instar larvae and the enrichment in the IPs using the *actin > Gal4* promoter. The left panel shows a band of about 120 KDa recognized by anti-HA antibodies and present only in the total lysates of control larvae (lane 1) or expressing HA-NOC1 (lane 2). In lanes 3 and 4 is shown the Ponceau staining relative to lanes 1 and 2. In the middle panel is shown the expression level of HA-NOC1 upon immunoblot with anti-HA antibodies from larvae lysate with buffer containing different concentrations of detergent and salt (lane 5–7). In the right panel is shown the immunoblot from the eluted material from the Seph-Prot-G conjugated with anti-HA antibody upon immunoprecipitation from lysates of larvae expressing HA-NOC1 using the *hsp70-heat-shock (hs)* inducible promoter after 1 h of heat-shock and 2 h of recovery. Lane 8 shows the immunoblot from lysates of control larvae *hs-w*^{1118,} while lane 9 shows the eluted from the immunoprecipitation from animals expressing *hs-HA-NOC1;* this represents 1/5 of the material used from the MS analysis. **(C)** Volcano plot highlighting all proteins enriched. The mean log2 ratio of hs-HA-NOC1 IPs versus control hs-w^{1118} IPs are plotted versus the corresponding *p*-values. 239 proteins significantly enriched (blue dots) with a *p*-value below 0.05 and log2-FC >1.5 thresholds were treated as putative NOC1 binding partners. The most representative interactors found for this analysis are indicated in the plot. **(D)** Schematic view of protein-protein interactions among NOC1 targets according to the STRING database (v.12). STRING protein-protein interaction analysis indicates the most prominent clusters with a medium confidence score of 0.4. Each node represents a protein, and each edge represents an interaction.

putative NOC1 binding partners (Supplementary List S1). The raw data are available via ProteomeXchange with identifier PXD047564. Results are illustrated by the volcano plot displaying the proteins significantly enriched in NOC1-IPs in light blue, with a fold change (FC) > 1.5 and *p*-value <0.05. To better characterize the NOC1 interactome, the list of putative interacting proteins was processed by STRING protein-protein interaction analysis, and clusters were identified in the resulting network using the Markov Clustering Algorithm (MCL) (Figure 2C). This analysis outlined a few interesting clusters of NOC1 interactors (Figure 2D). The most relevant is Cluster1, which includes NOC2 and NOC3 (Supplementary Table S1, and Volcano plot Figure 2C). The same cluster also includes nucleolar proteins such as Fibrillarin (Fib), an rRNA O-methyltransferase, and l(3)07882 required for the processing of the pre-rRNAs, Novel nucleolar proteins (Non1 and Non3) involved in the biogenesis of the 60S subunits and needed for the assembling of the mitotic spindle, like Nucleostemin 1 (Ns1), required for the release of the 60S ribosomal subunit, mushroom body miniature (mbm) involved in ribosome biogenesis. Others non nucleolar proteins, like the CG13096, a homolog of human Ribosomal L1 domain-containing protein (RSLD1), the CG6724, a putative homolog of WRD12 required for the maturation of rRNAs and the formation of the large ribosomal subunit, Nnp, and Tsr1 described for the processing of pre-rRNAs and the control of RNA maturation. Notably, we also found in the interactome the DEAD-box RNA helicases pitchoune (pit) (Zaffran et al., 1998) and bel, *Drosophila* homologs of MrDb (Grandori et al., 1996) and *DDX3* (Liao et al., 2019) respectively. Interestingly, few of these proteins, such as pit (Zaffran et al., 1998), modulo (mod) (Perrin et al., 2003), Nnp (Nnp1) (Hulf et al., 2005), and peter pan (ppan) (Zielke et al., 2022), have been previously identified as putative direct targets of MYC specifically in the context of controlling cell growth and proliferation.

This analysis also found a highly represented cluster containing Ythdc1 (YTH domain RNA Binding Protein C1), Flacc (Fl(2)d-associated protein), and splenito (nito). Ythdc1 is a conserved nuclear m^{6}A "reader" protein that mediates the incorporation of methylated mRNAs into the nuclear export pathway (Roundtree et al., 2017; Shi et al., 2021). Interestingly, Flacc was found to be associated with female lethal (Fl(2)d), a protein homolog of Wilms'-tumor-1-associated protein (WTAP) (Penn et al., 2008), that was

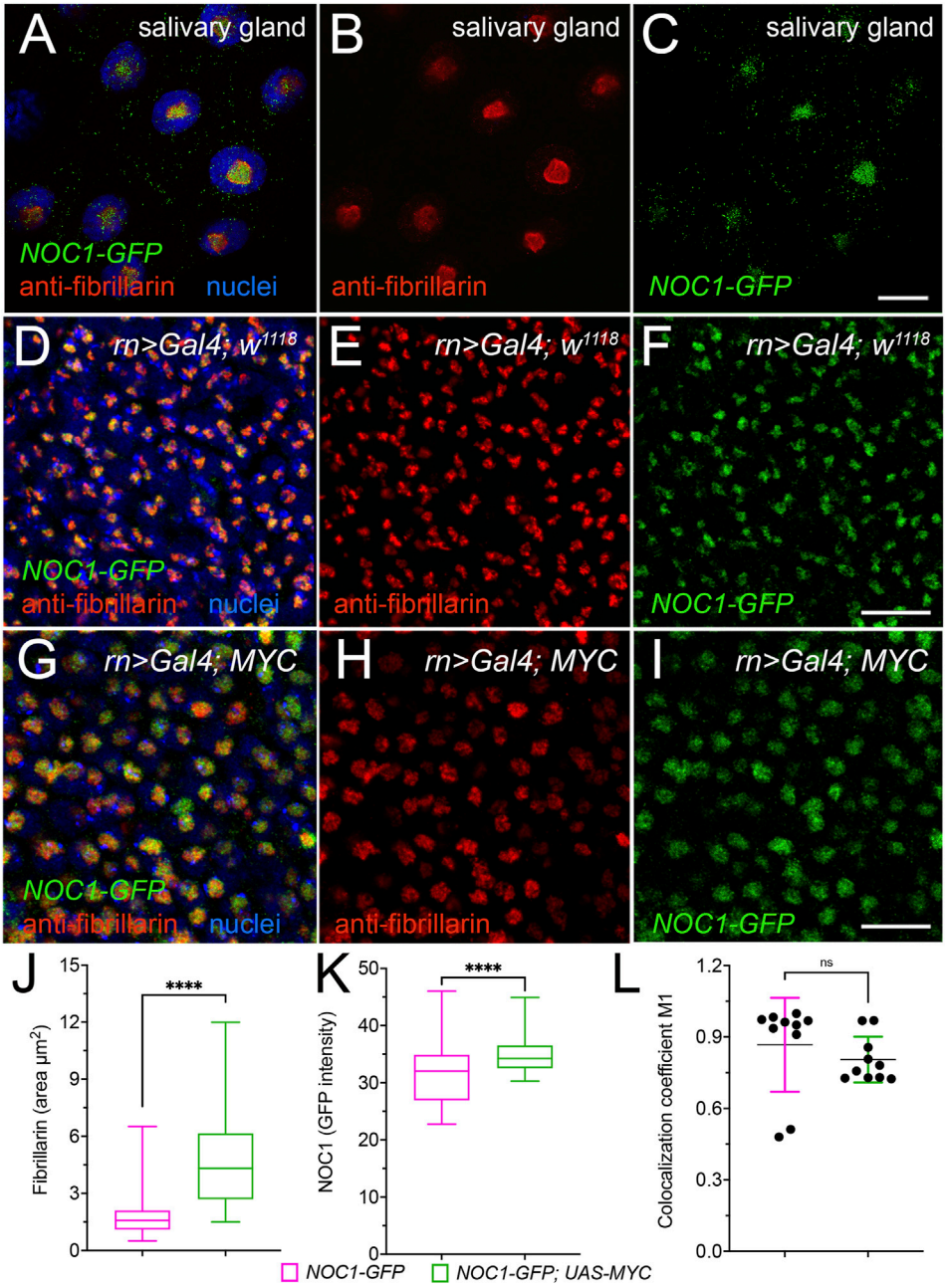

FIGURE 3
NOC1 nucleolar expression increases with MYC induction. **(A–C)** Confocal images of the cells from the salivary glands showing the endogenous fibrillarin expression in the nucleolus and its colocalization with NOC1-GFP, visualized with anti-fibrillarin **(B)** and anti-GFP **(C)** antibodies to visualize NOC1-GFP fusion protein (otherwise too low to detect directly), with nuclei stained in blue in A. **(D–F)** Cells of the wing imaginal discs showing endogenous fibrillarin **(E)** and NOC1-GFP expression **(F)**, and their colocalization in D. **(G–I)** Cells of the wing imaginal discs expressing *UAS-MYC,* using the *rotund-Gal4* promoter, stained for fibrillarin **(H)** and NOC1-GFP **(I)**. In **(G)**, they merged images with nuclei stained with Hoechst (blue). Note that the nucleolus size increases by MYC expression (see also Figure 6A for quantification). **(J)** Analysis of the fibrillarin area in cells of the wing imaginal disc of *NOC1-GFP; rn > w*^{1118} animals or expressing *NOC1-GFP; rn > UAS-MYC*. **(K)** Analysis of the GFP intensity relative to NOC1 expression in the nucleolus area in cells of the wing imaginal disc of *NOC1-GFP; rn > w*^{1118} animals or expressing *NOC1-GFP; rn > UAS-MYC*. **(L)** Coefficient of localization between NOC1 and fibrillarin in cells from control animals (*NOC1-GFP; rn > w*^{1118}) or expressing MYC (*NOC1-GFP; rn > UAS-MYC*). This analysis was performed using the Coloc2 plug-in of the Fiji software coloc2, and *p*-values calculated based on raw values that represent Manders' colocalization coefficient (with automatic Costes threshold). Scale bars in Figure C represent 20 µm, and in Figures F and D, 10 µm. The experiments were repeated at least three times, and the statistical analysis among the various genotypes was examined by Student's t-test, and *p* values are indicated with asterisks **** = $p < 0.0001$.

isolated in complexes with Snf (Penn et al., 2008), a component of U1 and U2 small nuclear ribonucleoproteins (snRNPs) that contained U2AF50, U2AF38, and U1-70K (small nuclear ribonucleoprotein 70K), which function in the regulation of the spliceosome. Notably, we observed an enrichment of the U2A proteins in our analysis (Supplementary Table S1), suggesting

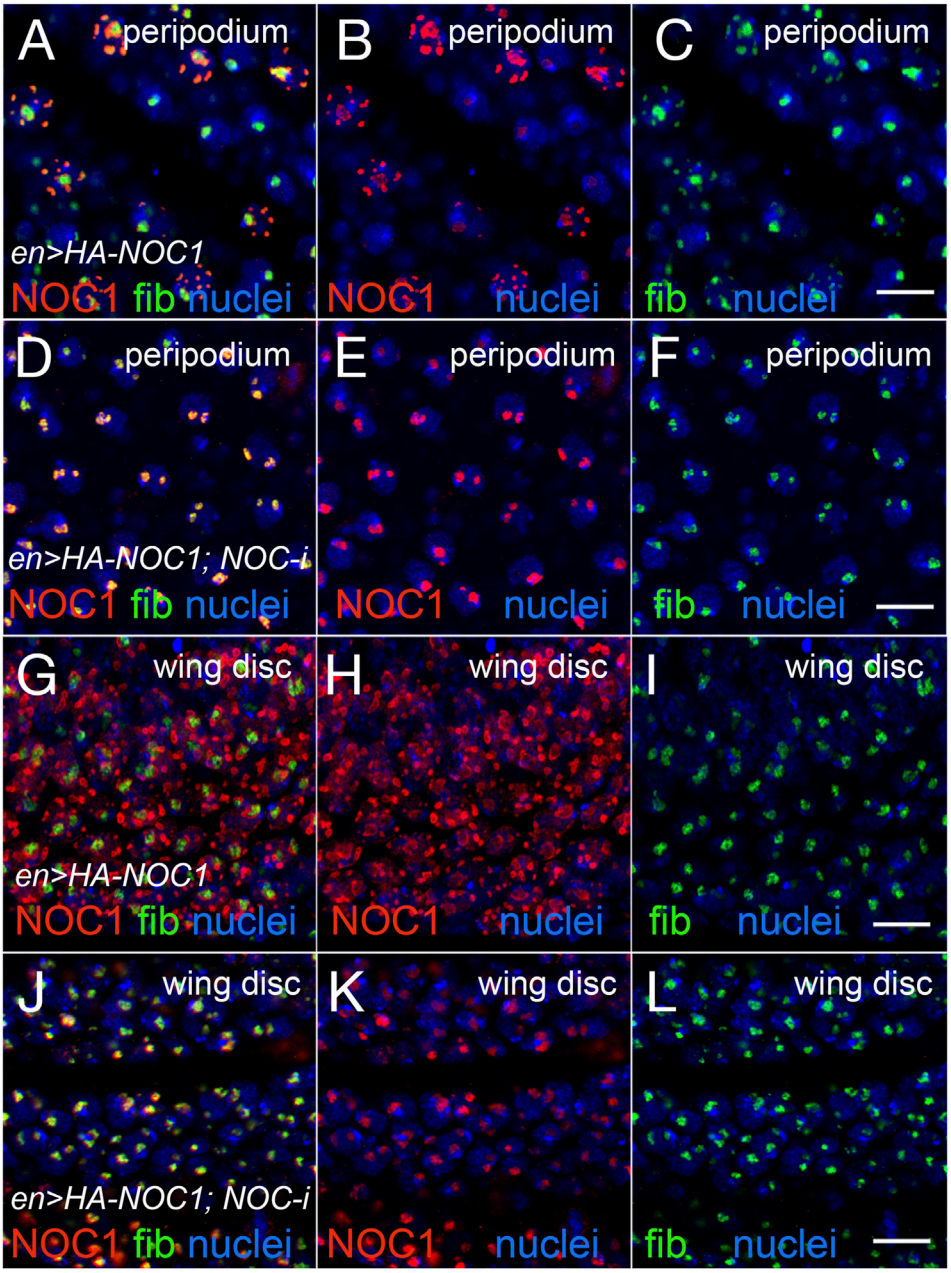

FIGURE 4
Expression of NOC1 induces extra nucleolar granules and enlargement of the nucleolus. **(A–C)** Confocal images of cells of the peripodium expressing HA-NOC1 alone or with NOC1-RNAi **(D–F)** using the *engrailed* promoter. **(G–L)** Images of cells from the imaginal disc expressing NOC1 alone **(G–I)** or with NOC1-RNAi (J–L). NOC1 and fibrillarin expression are visualized by immunofluorescence using anti-HA (red) and anti-fibrillarin (green) antibodies, respectively. Hoechst is used to visualize the nuclei. Scale bars represent 10 μm.

that NOC1 may play a key role in RNA splicing by linking the U1 snRNP particle to regulatory RNA-binding proteins and in the control of nuclear export via Ythdc1.

3.3 NOC1 expression in the nucleolus increases upon MYC induction

We previously showed that endogenous NOC1 colocalizes with fibrillarin in the nucleolus (Destefanis et al., 2022). Here, we confirm the co-localization of endogenous NOC1-GFP, expressed as GFP fusion protein (NOC1-GFP) under its endogenous promoter (Kudron et al., 2018) with fibrillarin. This is seen in the gigantic nucleolus of the salivary gland cells (Figures 3A–C) and the nucleolus of cells from the wing imaginal disc (Figures 3D–F). Furthermore, expression of MYC in cells of the wing imaginal disc, using *rotund-Gal4* promoter (Figures 3G–I), significantly increases the fibrillarin area in the nucleolus (Figure 3J) and also the fluorescence intensity of NOC1-GFP (Figure 3K), which are both direct transcriptional targets of MYC. However, statistical analysis

indicates that the coefficient of localization between NOC1 and fibrillarin does not change upon MYC expression, as shown from data in cells from control animals (*NOC1-GFP; rn > w*^{1118}) compared to that from cells expressing MYC (*NOC1-GFP; rn > UAS-MYC*) (Figure 3L), indicating that MYC promotes an increase in nucleolar size and of NOC1-GFP expression in the nucleolus.

3.4 NOC1 overexpression induces the formation of large nuclear granules and enlarged nucleoli that co-localize with fibrillarin

We previously reported that ectopic expression of NOC1 results in nucleolar morphology changes (Destefanis et al., 2022). To analyze how the ectopic expression of NOC1 could influence nucleolar morphology, we overexpressed the HA-tagged version of NOC1 in cells of the wing imaginal discs using the *engrailed-Gal4* promoter. *Engrailed* is expressed in both the columnar epithelium forming the wing imaginal disc and in the giant cells of the peripodium, a squamous epithelium adjacent to the columnar epithelium of the wing discs (Pallavi and Shashidhara, 2005; Smith-Bolton, 2016). Analysis of NOC1 expression in these cells, by immunostaining using an anti-HA antibody, revealed in the nucleus the presence of large granules containing HA-NOC1 and an enlargement of the size of the nucleolus, where NOC1 is visibly expressed. The granules are more easily distinct and visible in the peripodium because of the gigantic size of these cells (Figures 4A, B) and with a lower resolution also in cells of the wing imaginal discs (Figures 4G, H). HA-NOC1 expression colocalizes with fibrillarin mainly in the nucleolus (Figures 4A, D, G, J), while in the granules, its expression was very low but detectable, particularly in the cells of the peripodium (Figure 4A). Co-expression of NOC1 with NOC1-RNAi visibly reduced both HA-NOC1 and the formation of the abnormal enlarged structures expression in both types of cells (Figures 3E, K). At the same time, the levels of fibrillarin in the nucleolus did not significantly change upon expression of NOC1-RNAi (compare Figure 4C with Figures 4F, I with Figure 4L).

3.5 NOC1 colocalizes in the nucleolus with Nucleostemin1 (Ns1) and its reduction affects nucleolar localization of Ns1

In the analysis of proteins that can functionally interact with NOC1, we identified Nucleostemin 1 (Ns1) (Lo and Lu, 2010), a nucleolar protein necessary for the transport of the 60S subunit that shuttles between the nucleolus and the nucleoplasm, and essential for the nucleolar organization (Rosby et al., 2009). To investigate whether NOC1 interacts with Ns1, we first analyzed their co-localization in wt control *w*^{1118} animals. Ns1-GFP (*UAS-Ns1-GFP*) was ectopically expressed alone or in combination with NOC1-RNAi or with NOC1-HA overexpression using the *patched-Gal4* promoter (Vegh and Basler, 2003). These data showed that when Ns1-GFP is expressed alone, it is primarily nucleolar, with about 7% of cells showing NS1-GFP staining outside the nucleolar region (Figure 5B). When NOC1-RNAi was expressed instead we observed a significant alteration in the subcellular localization of Ns1-GFP, with a 30% increased of cells that showed NS1 localization in the nucleoplasm (Figure 5D). Analysis of NOC1 colocalization with Ns1, using anti HA immunostaining, showed the presence of both proteins in the nucleolus and also in the large granules (Figure 5F). These data together with MS results suggest that both Ns1 and NOC1 proteins may be part of a multi proteins complex that is necessary to keep nucleolar integrity (MODEL).

3.6 MYC cooperates with NOC1 to increase nucleolus size

We then analyzed if increasing the rate of protein synthesis by overexpressing MYC could have an effect on the size of the nucleolus or of the NOC1 granules, assuming that they might function as storage of ribosomal factors produced in excess by NOC1 overexpression. We examined and quantified the area of fibrillarin expression in the nucleolus in cells of the wing imaginal discs from control animals or expressing NOC1 or MYC alone, and a combination of both. These analyses confirmed that the expression of MYC or NOC1 alone significantly affects the nucleolar size (Figures 6A–C), with their co-expression that further increases the nucleolus size (Figures 6F–H). A more exhaustive analysis of the immunofluorescence images shows that NOC1-HA is found predominantly localized at the Dense Fibrillarin Center (DFC), that is, the external layer of the Fibrillarin Center (FC), while fibrillarin is in the center (Figures 6C–E). In the presence of MYC this effect of their localization is ever more pronounced (Figures 6F–H). From these experiments, we can also conclude that the granules are maintaining the structure with the core of fibrillarin (Red) with NOC1 surrounding the area (green), both in the condition of NOC expression alone or in combination with MYC (Figures 6E, F). In addition, we analyzed and found a high level of colocalization between NOC1 and *Drosophila* vito protein (Supplementary Figure S1). Nol12/vito is an RNA DNA binding protein homologous to human Nol12 and yeast Rrp17p (Scott et al., 2017). It was shown necessary for the processing of the 60S ribosomal subunits in yeast (Oeffinger et al., 2009), and required in flies for proper formation of nucleolar architecture in MYC-induced growth (Marinho et al., 2011). The two proteins colocalize in the nucleolus and the nuclear “granules” in cells of the wing imaginal disc. In these experiments, NOC1-HA localizes in the DFC of the nucleolus while Nol12-GFP is more present in the FC (S1 panel C); similarly, it was reported for human Hela cells, that Nol12 co-localizes with fibrillarin and was also expressed in the DFC (Scott et al., 2017). We should mention that the pattern of expression described for NOC1 in these experiments recapitulates the expression of nucleophosmin, which surrounds the core-shell architecture of fibrillarin in the center of the nucleoli (Lafontaine et al., 2021), further supporting the localization of NOC1 within the nucleolus.

4 Discussion

The nucleolus is a critical subcellular compartment involved in ribosome biogenesis, and proteins like NOC1 play essential roles in

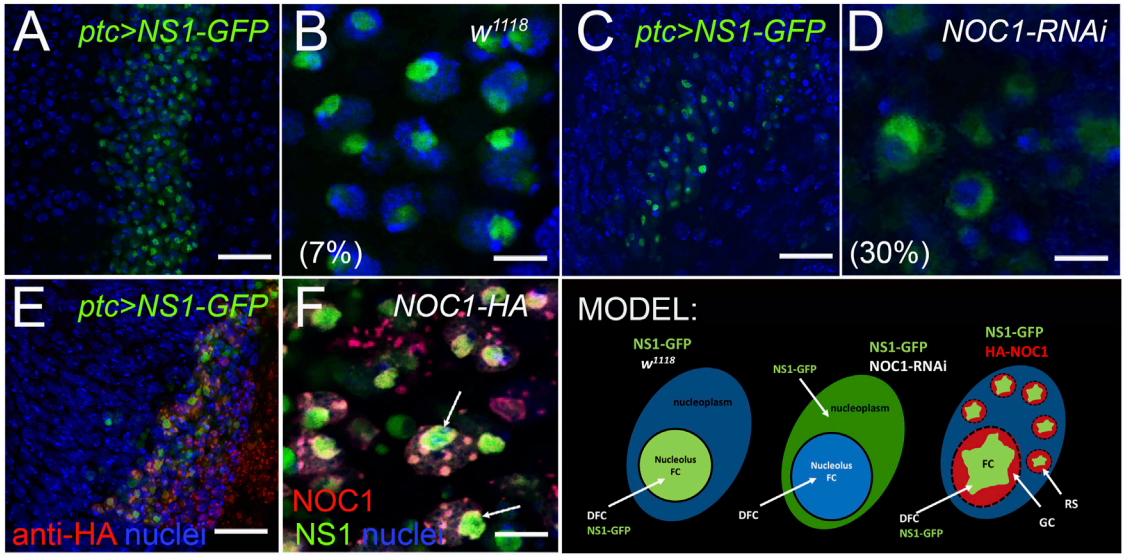

FIGURE 5
Reduction of NOC1 affects Nulceostemin1 (Ns1) nucleolar localization. Confocal images of cells from the wing imaginal disc expressing NOC1 (*UAS-HA-NOC1*) and Ns1 (*UAS-Ns1-GFP*) using the *patched-Gal4* promoter. **(A,B) (A)** shows a low-resolution image of the cells of the wing imaginal disc where patched is expressed as a stripe of cells along the Dorsal Ventral axis (Johnson et al., 1995). NS1-expressing cells are visible by GFP expression. **(B)** higher magnification of figure in panel A, showing expression of Ns1-GFP in the nucleolus. **(C)** low-resolution image of the cells expressing Ns1-GFP together with NOC1-RNAi. **(D)** higher magnification of the figure in panel **(C)**. In the parenthesis is reported the percentage of cells with NS1-GFP found perinucleolar or in the nucleoplasm (see also MODEL). **(E)** low-resolution image of the cells of the wing imaginal disc expressing Ns1-GFP together with NOC1-HA. **(F)** higher magnification of the figure in panel E shows HA-NOC1 that co-localizes with Ns1-GFP. This colocalization is visible in the nucleolus and (Arrows). also in the small granules characteristic of NOC1-HA overexpression. Scale bars in A-C and E represent 20 μm, and B-D and F represent 5 μm. MODEL suggesting the functional interaction of Ns1 with NOC1 in the nucleolus and describing the nucleolus organization as FC, Fibrillar Center; DFC, Dense Fibrillar Components; GC, Granular Center (Lam et al., 2005). GS, Granular Structures visualized by NOC1 overexpression.

this process. The conservation of NOC1 function across these diverse organisms, from yeast (*S.ce*) *Arabidopsis, Drosophila* (Milkereit et al., 2001; Li et al., 2009; de Bossoreille et al., 2018; Destefanis et al., 2022) and to some extent humans (Barbieri et al., 2017) (our unpublished data), indicates the fundamental role of this nucleolar factor in controlling basic and essential processes during ribosome biogenesis.

We have recently characterized the function of the sole nucleolar *NOC1* gene in *Drosophila* and show that it is necessary for proper rRNA processing and maturation, while its downregulation reduces protein synthesis and is detrimental to organ and animal growth (Destefanis et al., 2022). Here, we characterized NOC1 as a *bona fide* MYC target gene and demonstrated that NOC1 is transcriptionally induced through a functional MYC-binding E-box sequence in the NOC1 promoter region (Figure 1). We then analyzed NOC1 interactome by MS analysis (Supplementary List S1) to identify how NOC1 functions in controlling ribosomes and in relation to MYC. These data reveal that NOC1 is in a complex with the nucleolar proteins NOC2 and NOC3, confirming previous data in yeast, and probably forms functional heterodimers necessary for the transport of the large ribosomal subunit during ribosome maturation (Milkereit et al., 2001; Hierlmeier et al., 2013). Our data also evidence an enrichment in NOC1-IPs of other nucleolar proteins, many of them such as fib, mod, nnp1, have been previously characterized as direct MYC's targets (Perrin et al., 2003; Hulf et al., 2005). In support of this last observation, we also found that in response to MYC, NOC1 expression and localization within the nucleolus is significantly increased, suggesting a direct functional response between MYC and NOC1 activities in this organelle. Notably, NOC1 overexpression leads to the formation of large nuclear granules and enlarged nucleoli, which co-localizes with nucleolar fibrillarin and Ns1. Additionally, we demonstrate that NOC1 expression is helping to keep Ns1 nucleolar localization, suggesting a role for NOC1 in maintaining nucleolar structure. Finally, the co-expression of NOC1 and MYC enhances the size of the nucleolus and the formation of abnormal granular structures within the nucleus containing NOC1, outlining another aspect where NOC1 and MYC activities may cooperate or be additive in controlling nucleolar dynamics.

Furthermore, our study also highlights NOC1 interaction with proteins relevant for RNA processing, modification, and splicing. Indeed, we found highly represented Ythdc1 and Flacc (Fl(2)d-associated protein) and spenito (nito), the flies homolog of the nucleolar large ribosomal subunit (60S) assembly factor RBM28 (Bryant et al., 2021). Notably, all these proteins are part of the mechanism that mediates N6-methyladenosine (m6A) methylation of mRNAs (Shi et al., 2021; Deng et al., 2023). Ythdc1 is a conserved nuclear m^{6}A "reader" protein that mediates the incorporation of methylated mRNAs for their nuclear export (Roundtree et al., 2017; Shi et al., 2021). Flacc is a component of the complex that mediates N6-methyladenosine methylation of mRNAs essential for mRNA splicing efficiency of pre-mRNA targets and a key regulator of Sxl (Sex-lethal) pre-mRNA splicing (Knuckles et al., 2018). Flacc is in

10.3389/fcell.2023.1293420

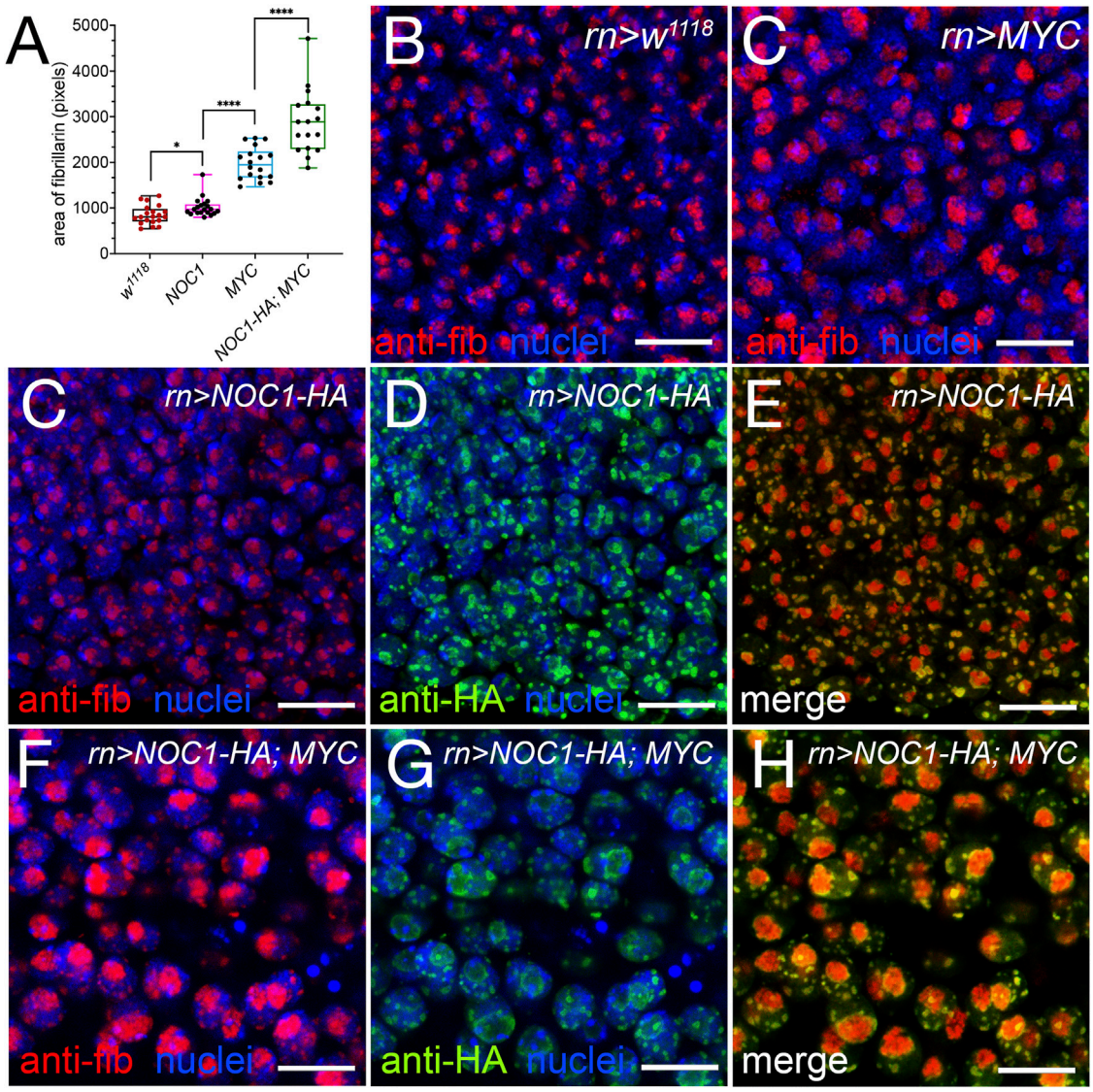

FIGURE 6
Expression of NOC1 and MYC enhances nucleolar size and morphology. **(A)** Graphic of the analysis of expression of fibrillarin in the nucleolus from cells of the wing imaginal discs, in animals expressing the indicated UAS-transgenes using the *rotund-Gal4* promoter. We considered the area stained by fibrillarin as a measurement of the nucleolar size and expressed it in pixels. These experiments were repeated at least twice, and the statistical analysis among the various genotypes was examined by Student's *t*-test, using the number of cells indicated in the graph. *p* values are indicated with asterisks * = $p < 0.05$, **** = $p < 0.0001$ respectively. **(B–H)** Confocal images of cells from the wing imaginal disc in control animals w^{1118} **(B)** and expressing MYC (*UAS-MYC*) **(C)**, NOC1 (*UAS-HA-NOC1*) **(C–E)**, or both NOC1 and MYC **(F–H)** using the *rotund-Gal4* promoter. Fibrillarin (red) and NOC1-HA (green) expression is visualized by immunofluorescence using anti-fibrillarin and anti-HA antibodies, respectively; nuclei are stained using Hoechst and visualized in blue. Scale bars represent 10 μm.

complex with female lethal (Fl(2)d), the *Drosophila* homolog of Wilms'-tumor-1-associated protein (WTAP) a component of human spliceosome (Zhou et al., 2002), and with Snf a component of U1/U2 small nuclear ribonucleoproteins (snRNPs) that contained U2AF50, U2AF38, and U1-70K necessary for splicing reaction of pre-mRNAs (Penn et al., 2008). Interestingly, we found an enrichment of these proteins in our analysis (Supplementary Table S1). Additionally, our data may suggest a potential link between NOC1 and snRNPs involved in regulating RNA-binding proteins and controlling mRNA nuclear export via m6A-dependent modifications by Ythdc1. This part highlights the complex and interconnected processes involved in gene expression regulation, from mRNA splicing to modifications. However, how NOC1 may control or be part of these mechanisms is still unclear.

Our previous analysis directly assessed the impact of NOC1 on pre-rRNA processing and cleavage and showed that its reduction induced an accumulation of pre-rRNA precursors (ITS1 and ITS2) (Destefanis et al., 2022). Similar data were found for the NOC1 homolog in yeast (Noc1p) using genetic screens and proteomic studies (Hierlmeier et al., 2013; Lebaron et al., 2013; Khoshnevis et al., 2019). However, we should comment on some crucial differences in the protein-interactome from our

experiments and those in yeast. Few reports in yeast annotated the Noc1p protein associated with Rrp5 (Ribosomal RNA Processing 5), a factor crucial for ribosome assembly that mediates the cleavage of the 35S pre-rRNA into the 18S rRNA, which is a critical step in the production of the small ribosomal subunit (Hierlmeier et al., 2013; Lebaron et al., 2013) and with Rcl1 (Ribosomal RNA Cleavage 1), another enzyme with a role in rRNA cleavage and processing (Khoshnevis et al., 2019). Both these proteins are conserved in flies. However, we did not find them in our NOC1-interactome analysis, even though Rrp5 was found in yeast bound to the pre-rRNA region of the ITS1 (Internal Transcriber Spacers-1) using protein crosslinking following by RNase treatment (Lebaron et al., 2013), and to interact with Noc1p and Noc2p (Hierlmeier et al., 2013) with a Noc1p-TAP purification system. We can explain these differences by hypothesizing that either the levels of Rrp5 and Rcl1 expressions are low in larvae compared to yeast or the use of different techniques and timing of purification of the protein used as bait in yeast compared to ours, i.e., during specific phases of RNA maturation and using Noc1p-TAP purification systems (Sailer et al., 2022). However, in the NOC1-interactome, we found NOC2 and NOC3, along with Nop53 (Rrp9) among others, described part of the Noc1p-yeast complex (Ohmayer et al., 2013), highlighting the significance of our preliminary studies in flies. It is important to acknowledge that studying the precise protein-interactome of NOC1 in *in vivo* can be challenging, and experimental conditions can limit the interpretation of results. In our case, conducting experiments at a single time point and under standard immunoprecipitation conditions may provide valuable insights into protein interactions but might not fully capture the dynamic and context-dependent nature of different NOC1's functions.

We found that NOC1 overexpression forms large granular structures containing NOC1, along with fibrillarin and Nucleostemin1 (Figure 4; Figure 5) and Nol12/viriato (Supplementary Figure S1). At the moment, we do not know the nature of these granules. We could hypothesize that these NOC1 granules work as dynamic and multifunctional structures regulating RNA metabolism and gene expression, including rRNA processing and transcription. These may include RNA stress granules formed during stress conditions to protect mRNAs from degradation or to control their translation (Putnam et al., 2023). This hypothesis is supported by our data that identify proteins of the DEAD-box RNA helicases family, such as pea/DXH8 and CG8611 pit, bel kurz, previously identified as components of RNA stress granules (Campos-Melo et al., 2021). This idea may also support the mechanism by which the abnormally large structures containing NOC1 and induced when MYC is overexpressed are the result of their synergistic effect in promoting cellular stress induced by a high protein synthesis or dysfunctions caused by the combination of MYC and NOC1 targets. Overexpression of MYC can lead to increased demand for ribosome biogenesis, and the presence of abnormal ribosomal intermediates due to NOC1 dysregulation can exacerbate this stress. This can result in nucleolar stress, activation of cellular stress responses, and potentially contribute to the insurgence of diseases.

Abnormal structures or extra nucleoli have significant implications in human diseases, particularly in cancer, where dysregulation of nucleolar functions is a hallmark of the disease (Orsolic et al., 2016; Penzo et al., 2019), and in ribosomopathies, a class of rare genetic diseases characterized by mutations in ribosomal proteins or components that impaired RNA translation associated with various clinical manifestations, including bone marrow failure, developmental disorders and an increased risk of cancer (Farley-Barnes et al., 2019; Kampen et al., 2020).

Finally, a few words about the human homolog of NOC1, called CEBPz (CCAAT/enhancer-binding protein zeta), a transcription factor so far associated with certain types of tumors. Notably, in acute myeloid leukemia (AML), CEBPz was shown to promote the m^6A modification of target mRNA transcripts, enhancing their translation (Barbieri et al., 2017; Hong et al., 2022). Thus, overexpression or downregulation of CEBPz in humans may also affect RNA processing, leading to defective translation. In support of this idea, the human gene rbm28, which we found in the NOC1 interactome, is responsible for the ribosomopathy-ane syndrome (Bryant et al., 2021), a rare genetic disorder caused by aberrant splicing in *RBM28* pre-mRNA. This, together with other indirect information on the potential role of NOC1/CEBPz in controlling alternative splicing, highlights the potential role of the human counterpart in the control of nucleolar processes that may cause genetic disorders.

Our research uses *Drosophila*, a simple and accessible model system, to identify novel conserved mechanisms to better understand MYC activity and its targets, including NOC1, in the context of RNA translation and ribosome biogenesis. The ultimate goal would be to identify specific targets within the translation machinery that small molecules or drugs can modulate for use in disease therapies.

Data availability statement

The datasets presented in this study can be found in online repositories. The names of the repository/repositories and accession number(s) can be found in the article/Supplementary Material.

Author contributions

VM: Conceptualization, Data curation, Formal Analysis, Investigation, Writing–review and editing. MR: Conceptualization, Data curation, Formal Analysis, Investigation, Methodology, Writing–review and editing. RB: Conceptualization, Data curation, Investigation, Methodology, Writing–review and editing. DP: Conceptualization, Data curation, Investigation, Methodology, Writing–review and editing, Formal Analysis, Software. FD: Conceptualization, Writing–review and editing. LA: Conceptualization, Writing–review and editing, Data curation, Investigation. GT: Investigation, Writing–review and editing, Formal Analysis, Software. TT: Software, Writing–review and editing, Data curation. PB: Data curation, Writing–review and editing, Conceptualization, Formal Analysis, Funding acquisition, Investigation, Methodology, Project administration, Supervision, Validation, Writing–original draft.

Funding

The author(s) declare that no financial support was received for the research, authorship, and/or publication of this article.

Acknowledgments

We thank the Mass Spectrometry and the Advanced Imaging facility at CIBIO. Stocks obtained from the Bloomington *Drosophila* Stock Center (NIH P40OD018537) were used in this study.

Conflict of interest

The authors declare that the research was conducted in the absence of any commercial or financial relationships that could be construed as a potential conflict of interest.

The author(s) declared that they were an editorial board member of Frontiers, at the time of submission. This had no impact on the peer review process and the final decision.

Publisher's note

Supplementary material

The Supplementary Material for this article can be found online at: https://www.frontiersin.org/articles/10.3389/fcell.2023.1293420/full#supplementary-material

References

Arabi, A., Wu, S., Ridderstrale, K., Bierhoff, H., Shiue, C., Fatyol, K., et al. (2005). c-Myc associates with ribosomal DNA and activates RNA polymerase I transcription. *Nat. Cell Biol.* 7, 303–310. doi:10.1038/ncb1225

Barbieri, I., Tzelepis, K., Pandolfini, L., Shi, J., Millan-Zambrano, G., Robson, S. C., et al. (2017). Promoter-bound METTL3 maintains myeloid leukaemia by m(6)A-dependent translation control. *Nature* 552, 126–131. doi:10.1038/nature24678

Bellosta, P., Hulf, T., Balla Diop, S., Usseglio, F., Pradel, J., Aragnol, D., et al. (2005). Myc interacts genetically with Tip48/Reptin and Tip49/Pontin to control growth and proliferation during Drosophila development. *Proc. Natl. Acad. Sci. U. S. A.* 102, 11799–11804. doi:10.1073/pnas.0408945102

Bryant, C. J., Lorea, C. F., De Almeida, H. L., Jr., Weinert, L., Vedolin, L., Pinto, E. V. F., et al. (2021). Biallelic splicing variants in the nucleolar 60S assembly factor RBM28 cause the ribosomopathy ANE syndrome. *Proc. Natl. Acad. Sci. U. S. A.* 118, e2017777118. doi:10.1073/pnas.2017777118

Campbell, K. J., and White, R. J. (2014). MYC regulation of cell growth through control of transcription by RNA polymerases I and III. *Cold Spring Harb. Perspect. Med.* 4, a018408. doi:10.1101/cshperspect.a018408

Campos-Melo, D., Hawley, Z. C. E., Droppelmann, C. A., and Strong, M. J. (2021). The integral role of RNA in stress granule formation and function. *Front. Cell Dev. Biol.* 9, 621779. doi:10.3389/fcell.2021.621779

Chiva, C., Olivella, R., Borras, E., Espadas, G., Pastor, O., Sole, A., et al. (2018). QCloud: a cloud-based quality control system for mass spectrometry-based proteomics laboratories. *PLoS One* 13, e0189209. doi:10.1371/journal.pone.0189209

De Bossoreille, S., Morel, P., Trehin, C., and Negrutiu, I. (2018). REBELOTE, a regulator of floral determinacy in *Arabidopsis thaliana*, interacts with both nucleolar and nucleoplasmic proteins. *FEBS Open Bio* 8, 1636–1648. doi:10.1002/2211-5463.12504

Deng, X., Qing, Y., Horne, D., Huang, H., and Chen, J. (2023). The roles and implications of RNA m(6)A modification in cancer. *Nat. Rev. Clin. Oncol.* 20, 507–526. doi:10.1038/s41571-023-00774-x

Destefanis, F., Manara, V., and Bellosta, P. (2020). Myc as a regulator of ribosome biogenesis and cell competition: a link to cancer. *Int. J. Mol. Sci.* 21, 4037. doi:10.3390/ijms21114037

Destefanis, F., Manara, V., Santarelli, S., Zola, S., Brambilla, M., Viola, G., et al. (2022). Reduction of nucleolar NOC1 leads to the accumulation of pre-rRNAs and induces Xrp1, affecting growth and resulting in cell competition. *J. Cell Sci.* 135, jcs260110. doi:10.1242/jcs.260110

Dorner, K., Ruggeri, C., Zemp, I., and Kutay, U. (2023). Ribosome biogenesis factors-from names to functions. *EMBO J.* 42, e112699. doi:10.15252/embj.2022112699

Farley-Barnes, K. I., Ogawa, L. M., and Baserga, S. J. (2019). Ribosomopathies: old concepts, new controversies. *Trends Genet.* 35, 754–767. doi:10.1016/j.tig.2019.07.004

Fernandez, P. C., Frank, S. R., Wang, L., Schroeder, M., Liu, S., Greene, J., et al. (2003). Genomic targets of the human c-Myc protein. *Genes Dev.* 17, 1115–1129. doi:10.1101/gad.1067003

Galletti, M., Riccardo, S., Parisi, F., Lora, C., Saqcena, M. K., Rivas, L., et al. (2009). Identification of domains responsible for ubiquitin-dependent degradation of dMyc by glycogen synthase kinase 3beta and casein kinase 1 kinases. *Mol. Cell Biol.* 29, 3424–3434. doi:10.1128/MCB.01535-08

Grandori, C., Gomez-Roman, N., Felton-Edkins, Z. A., Ngouenet, C., Galloway, D. A., Eisenman, R. N., et al. (2005). c-Myc binds to human ribosomal DNA and stimulates transcription of rRNA genes by RNA polymerase I. *Nat. Cell Biol.* 7, 311–318. doi:10.1038/ncb1224

Grandori, C., Mac, J., Siebelt, F., Ayer, D. E., and Eisenman, R. N. (1996). Myc-Max heterodimers activate a DEAD box gene and interact with multiple E box-related sites *in vivo*. *EMBO J.* 15, 4344–4357. doi:10.1002/j.1460-2075.1996.tb00808.x

Grewal, S. S., Li, L., Orian, A., Eisenman, R. N., and Edgar, B. A. (2005). Myc-dependent regulation of ribosomal RNA synthesis during Drosophila development. *Nat. Cell Biol.* 7, 295–302. doi:10.1038/ncb1223

Hierlmeier, T., Merl, J., Sauert, M., Perez-Fernandez, J., Schultz, P., Bruckmann, A., et al. (2013). Rrp5p, Noc1p and Noc2p form a protein module which is part of early large ribosomal subunit precursors in *S. cerevisiae*. *Nucleic Acids Res.* 41, 1191–1210. doi:10.1093/nar/gks1056

Hong, J., Xu, K., and Lee, J. H. (2022). Biological roles of the RNA m(6)A modification and its implications in cancer. *Exp. Mol. Med.* 54, 1822–1832. doi:10.1038/s12276-022-00897-8

Hulf, T., Bellosta, P., Furrer, M., Steiger, D., Svensson, D., Barbour, A., et al. (2005). Whole-genome analysis reveals a strong positional bias of conserved dMyc-dependent E-boxes. *Mol. Cell Biol.* 25, 3401–3410. doi:10.1128/MCB.25.9.3401-3410.2005

Johnson, R. L., Grenier, J. K., and Scott, M. P. (1995). Patched overexpression alters wing disc size and pattern: transcriptional and post-transcriptional effects on hedgehog targets. *Development* 121, 4161–4170. doi:10.1242/dev.121.12.4161

Kampen, K. R., Sulima, S. O., Vereecke, S., and De Keersmaecker, K. (2020). Hallmarks of ribosomopathies. *Nucleic Acids Res.* 48, 1013–1028. doi:10.1093/nar/gkz637

Khoshnevis, S., Liu, X., Dattolo, M. D., and Karbstein, K. (2019). Rrp5 establishes a checkpoint for 60S assembly during 40S maturation. *RNA* 25, 1164–1176. doi:10.1261/rna.071225.119

Kim, H. J., Kim, T., Hoffman, N. J., Xiao, D., James, D. E., Humphrey, S. J., et al. (2021). PhosR enables processing and functional analysis of phosphoproteomic data. *Cell Rep.* 34, 108771. doi:10.1016/j.celrep.2021.108771

Knuckles, P., Lence, T., Haussmann, I. U., Jacob, D., Kreim, N., Carl, S. H., et al. (2018). Zc3h13/Flacc is required for adenosine methylation by bridging the mRNA-binding factor Rbm15/Spenito to the m(6)A machinery component Wtap/Fl(2)d. *Genes Dev.* 32, 415–429. doi:10.1101/gad.309146.117

Koh, C. M., Gurel, B., Sutcliffe, S., Aryee, M. J., Schultz, D., Iwata, T., et al. (2011). Alterations in nucleolar structure and gene expression programs in prostatic neoplasia are driven by the MYC oncogene. *Am. J. Pathol.* 178, 1824–1834. doi:10.1016/j.ajpath.2010.12.040

Kudron, M. M., Victorsen, A., Gevirtzman, L., Hillier, L. W., Fisher, W. W., Vafeados, D., et al. (2018). The ModERN resource: genome-wide binding profiles for hundreds of Drosophila and *Caenorhabditis elegans* transcription factors. *Genetics* 208, 937–949. doi:10.1534/genetics.117.300657

Lafontaine, D. L. J., Riback, J. A., Bascetin, R., and Brangwynne, C. P. (2021). The nucleolus as a multiphase liquid condensate. *Nat. Rev. Mol. Cell Biol.* 22, 165–182. doi:10.1038/s41580-020-0272-6

Lam, Y. W., Trinkle-Mulcahy, L., and Lamond, A. I. (2005). The nucleolus. *J. Cell Sci.* 118, 1335–1337. doi:10.1242/jcs.01736

Lebaron, S., Segerstolpe, A., French, S. L., Dudnakova, T., De Lima Alves, F., Granneman, S., et al. (2013). Rrp5 binding at multiple sites coordinates pre-rRNA processing and assembly. *Mol. Cell* 52, 707–719. doi:10.1016/j.molcel.2013.10.017

Li, N., Yuan, L., Liu, N., Shi, D., Li, X., Tang, Z., et al. (2009). SLOW WALKER2, a NOC1/MAK21 homologue, is essential for coordinated cell cycle progression during female gametophyte development in Arabidopsis. *Plant Physiol.* 151, 1486–1497. doi:10.1104/pp.109.142414

Liao, S. E., Kandasamy, S. K., Zhu, L., and Fukunaga, R. (2019). DEAD-box RNA helicase Belle posttranscriptionally promotes gene expression in an ATPase activity-dependent manner. *RNA* 25, 825–839. doi:10.1261/rna.070268.118

Lo, D., and Lu, H. (2010). Nucleostemin: another nucleolar "Twister" of the p53-MDM2 loop. *Cell Cycle* 9, 3227–3232. doi:10.4161/cc.9.16.12605

Marinho, J., Casares, F., and Pereira, P. S. (2011). The Drosophila Nol12 homologue viriato is a dMyc target that regulates nucleolar architecture and is required for dMyc-stimulated cell growth. *Development* 138, 349–357. doi:10.1242/dev.054411

Migeon, J. C., Garfinkel, M. S., and Edgar, B. A. (1999). Cloning and characterization of peter pan, a novel Drosophila gene required for larval growth. *Mol. Biol. Cell* 10, 1733–1744. doi:10.1091/mbc.10.6.1733

Milkereit, P., Gadal, O., Podtelejnikov, A., Trumtel, S., Gas, N., Petfalski, E., et al. (2001). Maturation and intranuclear transport of pre-ribosomes requires Noc proteins. *Cell* 105, 499–509. doi:10.1016/s0092-8674(01)00358-0

Oeffinger, M., Zenklusen, D., Ferguson, A., Wei, K. E., El Hage, A., Tollervey, D., et al. (2009). Rrp17p is a eukaryotic exonuclease required for 5' end processing of Pre-60S ribosomal RNA. *Mol. Cell* 36, 768–781. doi:10.1016/j.molcel.2009.11.011

Ohmayer, U., Gamalinda, M., Sauert, M., Ossowski, J., Poll, G., Linnemann, J., et al. (2013). Studies on the assembly characteristics of large subunit ribosomal proteins in S. cerevisae. *PLoS One* 8, e68412. doi:10.1371/journal.pone.0068412

Orian, A., Van Steensel, B., Delrow, J., Bussemaker, H. J., Li, L., Sawado, T., et al. (2003). Genomic binding by the Drosophila Myc, Max, Mad/Mnt transcription factor network. *Genes Dev.* 17, 1101–1114. doi:10.1101/gad.1066903

Orsolic, I., Jurada, D., Pullen, N., Oren, M., Eliopoulos, A. G., and Volarevic, S. (2016). The relationship between the nucleolus and cancer: current evidence and emerging paradigms. *Semin. Cancer Biol.* 37-38, 36–50. doi:10.1016/j.semcancer.2015.12.004

Pallavi, S. K., and Shashidhara, L. S. (2005). Signaling interactions between squamous and columnar epithelia of the Drosophila wing disc. *J. Cell Sci.* 118, 3363–3370. doi:10.1242/jcs.02464

Parisi, F., Riccardo, S., Zola, S., Lora, C., Grifoni, D., Brown, L. M., et al. (2013). dMyc expression in the fat body affects DILP2 release and increases the expression of the fat desaturase Desat1 resulting in organismal growth. *Dev. Biol.* 379, 64–75. doi:10.1016/j.ydbio.2013.04.008

Penn, J. K., Graham, P., Deshpande, G., Calhoun, G., Chaouki, A. S., Salz, H. K., et al. (2008). Functioning of the Drosophila Wilms'-tumor-1-associated protein homolog, Fl(2)d, in Sex-lethal-dependent alternative splicing. *Genetics* 178, 737–748. doi:10.1534/genetics.107.081679

Penzo, M., Montanaro, L., Trere, D., and Derenzini, M. (2019). The ribosome biogenesis-cancer connection. *Cells* 8. doi:10.3390/cells8010055

Perrin, L., Benassayag, C., Morello, D., Pradel, J., and Montagne, J. (2003). Modulo is a target of Myc selectively required for growth of proliferative cells in Drosophila. *Mech. Dev.* 120, 645–655. doi:10.1016/s0925-4773(03)00049-2

Putnam, A., Thomas, L., and Seydoux, G. (2023). RNA granules: functional compartments or incidental condensates? *Genes Dev.* 37, 354–376. doi:10.1101/gad.350518.123

Rosby, R., Cui, Z., Rogers, E., Delivron, M. A., Robinson, V. L., and Dimario, P. J. (2009). Knockdown of the Drosophila GTPase nucleostemin 1 impairs large ribosomal subunit biogenesis, cell growth, and midgut precursor cell maintenance. *Mol. Biol. Cell* 20, 4424–4434. doi:10.1091/mbc.e08-06-0592

Roundtree, I. A., Luo, G. Z., Zhang, Z., Wang, X., Zhou, T., Cui, Y., et al. (2017). YTHDC1 mediates nuclear export of N(6)-methyladenosine methylated mRNAs. *Elife* 6, e31311. doi:10.7554/eLife.31311

Sailer, C., Jansen, J., Sekulski, K., Cruz, V. E., Erzberger, J. P., and Stengel, F. (2022). A comprehensive landscape of 60S ribosome biogenesis factors. *Cell Rep.* 38, 110353. doi:10.1016/j.celrep.2022.110353

Sanghai, Z. A., Piwowarczyk, R., Broeck, A. V., and Klinge, S. (2023). A co-transcriptional ribosome assembly checkpoint controls nascent large ribosomal subunit maturation. *Nat. Struct. Mol. Biol.* 30, 594–599. doi:10.1038/s41594-023-00947-3

Schlosser, I., Holzel, M., Murnseer, M., Burtscher, H., Weidle, U. H., and Eick, D. (2003). A role for c-Myc in the regulation of ribosomal RNA processing. *Nucleic Acids Res.* 31, 6148–6156. doi:10.1093/nar/gkg794

Scott, D. D., Trahan, C., Zindy, P. J., Aguilar, L. C., Delubac, M. Y., Van Nostrand, E. L., et al. (2017). Nol12 is a multifunctional RNA binding protein at the nexus of RNA and DNA metabolism. *Nucleic Acids Res.* 45, 12509–12528. doi:10.1093/nar/gkx963

Shi, R., Ying, S., Li, Y., Zhu, L., Wang, X., and Jin, H. (2021). Linking the YTH domain to cancer: the importance of YTH family proteins in epigenetics. *Cell Death Dis.* 12, 346. doi:10.1038/s41419-021-03625-8

Smith-Bolton, R. (2016). Drosophila imaginal discs as a model of epithelial wound repair and regeneration. *Adv. Wound Care (New Rochelle)* 5, 251–261. doi:10.1089/wound.2014.0547

Van Riggelen, J., Yetil, A., and Felsher, D. W. (2010). MYC as a regulator of ribosome biogenesis and protein synthesis. *Nat. Rev. Cancer* 10, 301–309. doi:10.1038/nrc2819

Vegh, M., and Basler, K. (2003). A genetic screen for hedgehog targets involved in the maintenance of the Drosophila anteroposterior compartment boundary. *Genetics* 163, 1427–1438. doi:10.1093/genetics/163.4.1427

Zaffran, S., Chartier, A., Gallant, P., Astier, M., Arquier, N., Doherty, D., et al. (1998). A Drosophila RNA helicase gene, pitchoune, is required for cell growth and proliferation and is a potential target of d-Myc. *Development* 125, 3571–3584. doi:10.1242/dev.125.18.3571

Zhou, Z., Licklider, L. J., Gygi, S. P., and Reed, R. (2002). Comprehensive proteomic analysis of the human spliceosome. *Nature* 419, 182–185. doi:10.1038/nature01031

Zhu, Y., Orre, L. M., Zhou Tran, Y., Mermelekas, G., Johansson, H. J., Malyutina, A., et al. (2020). DEqMS: a method for accurate variance estimation in differential protein expression analysis. *Mol. Cell Proteomics* 19, 1047–1057. doi:10.1074/mcp.TIR119.001646

Zielke, N., Vaharautio, A., Liu, J., Kivioja, T., and Taipale, J. (2022). Upregulation of ribosome biogenesis via canonical E-boxes is required for Myc-driven proliferation. *Dev. Cell* 57, 1024–1036.e5. doi:10.1016/j.devcel.2022.03.018